01 Jan 1990

Boundary Element-Image Method Approach to Seismic Modeling

Richard E. DuBroff
Missouri University of Science and Technology, red@mst.edu

Recommended Citation

R. E. DuBroff, "Boundary Element-Image Method Approach to Seismic Modeling," *Journal of Geophysical Research*, vol. 95, no. B2, pp. 1215 - 1222, Wiley; American Geophysical Union, Jan 1990.
The definitive version is available at https://doi.org/10.1029/JB095iB02p01215

JOURNAL OF GEOPHYSICAL RESEARCH, VOL. 95, NO. B2, PAGES 1215–1222, FEBRUARY 10, 1990

Boundary Element-Image Method Approach to Seismic Modeling

R. E. DuBroff

Department of Electrical Engineering, University of Missouri at Rolla

The boundary element-image method is proposed as a method for generating synthetic seismograms in a system of piecewise homogeneous layers. In contrast with many other methods (such as finite difference) in which the boundary conditions are represented simply by a change of material properties, the present approach uses the boundary conditions explicitly in order to develop a system of integral equations. As in the indirect boundary element method, the scattered seismic waves are presumed to result from the action of fictitious sources. However, as in the image method, these fictitious sources are located outside of the domain through which the scattered waves propagate. This combination of the image and boundary element methods thereby avoids introducing additional singularities (in the form of fictitious sources) into the wave equation for the scattered waves. Although this method can be formulated in a general way, specific computational advantages occur when the basis and testing functions are chosen as harmonically related complex sinusoids. Physically, this corresponds to a plane wave expansion of the scattered waves. Computationally, when considering piecewise linear interfaces, this results in a (possibly) large system of simultaneous algebraic equations having matrix elements which can be calculated analytically. This method is applied to the reflection of seismic waves from a V- shaped reflector subjected to two different incident waves: a plane wave and a cylindrical wave created by a line source. The synthetic seismograms for both cases are presented (in the form of time sections) and then processed in an attempt to reconstruct the geometry of the reflector (in the form of a depth section).

1. Introduction

Several methods of seismic modeling have been developed over the past decade. Generally, these methods can be categorized as either wave equation methods, which utilize a numerical approach to the solution of differential equations, or ray methods, which primarily utilize a geometrical approach. While there are some methods which correspond to a hybrid approach, the present description falls within the category of wave equation methods.

One particular approach to wave equation modeling is the finite difference approach, in which the various differential operators in the acoustic wave equation are replaced with differencing operators, thereby reducing (and also approximating) the wave equation directly by a system of simultaneous linear algebraic equations [*Claerbout*, 1976; *Kelly et al.*, 1978]. While the finite difference approach has the intuitive appeal of replacing various derivatives with their finite difference approximations, it can be shown [e.g., *Zienkiewicz*, 1977; *Marfurt*, 1984] that the finite difference method can be derived as a special case of the method of weighted residuals. This general method also includes the finite element method.

In both the finite difference and finite element methods the unknown function is defined throughout the volume of the scattering object. The present approach, in contrast, is more closely allied with the boundary element method [*Brebbia*, 1978] in which the unknown function is defined over the surface (or surfaces) of the scattering object. The use of direct boundary integral methods for acoustic scattering has been discussed, for example, by *Schuster and Smith* [1985]. As is the case in the boundary element method, the present approach results in a set of integral equations. The present approach differs from the conventional boundary element approach, however, by introducing a set of auxiliary surfaces over which the unknown functions are defined. As these auxiliary surfaces are external to the scattering volume, they do not introduce any additional singularities in the wave equation for the region internal to the scattering volume. An approach of this sort has recently been proposed for the case of transverse electric (TE) electromagnetic scattering in cylindrical geometry by *Leviatan et al.* [1988]. In the present case, two dimensional boundaries which do not form closed curves will be considered.

Paper number 89JB03041.
0148-0227/90/89JB-03041$05.00

As shown in Figure 1, the geological model will be presumed to consist of some number of uniform homogeneous layers separated by interfaces (or boundaries). While layers 1 and N are semi-infinite, all of the intervening layers are bounded. Specifically, the top of layer m will be denoted by the surface $\Upsilon_m^{(1)}(\vec{r})$, while the bottom of layer m will be denoted by the surface $\Upsilon_m^{(2)}(\vec{r})$. Since the top of layer m corresponds to the bottom of of layer m-1, the surface $\Upsilon_m^{(1)}(\vec{r})$ is the same as the surface $\Upsilon_{m-1}^{(2)}(\vec{r})$, and as a result, each interface has two names.

2. Description of Method

Referring now to Figure 2, let layer m be bounded by the surface Ω_m^- above and the surface Ω_m^+ below. In this case, the surface Ω_m^- corresponds to $Z = Z_{0m}^-$, while Ω_m^+ corresponds to $Z = Z_{0m}^+$. On the upper bounding surface the assumed distribution of sources is given by the function $A_m^+(\vec{r}', \omega)$, while $A_m^-(\vec{r}', \omega)$ corresponds to the assumed distribution of sources on the lower bounding surface.

In this method the pressure function $P_m(\vec{r}, \omega)$ associated with the passage of a seismic wave is presumed to result from the action of distributed sources located on the surfaces which bound layer m. For a layer of finite thickness ($1 < m < N$) this allows the pressure function to be represented as

$$P_m(\vec{r}, \omega) = \iint_{\Omega_m^+} A_m^+(\vec{r}', \omega)\, G_m(\vec{r} \mid \vec{r}')\, d\Omega_m^+(\vec{r}') + \iint_{\Omega_m^-} A_m^-(\vec{r}', \omega)\, G_m(\vec{r} \mid \vec{r}')\, d\Omega_m^-(\vec{r}') \quad (1)$$

when $\vec{r}$ is in layer m and where $G_m(\vec{r} \mid \vec{r}')$ is the Green's function due to a point source at $\vec{r}'$.

The same equation can be applied to the first layer ($m = 1$) by setting the second term to zero and to the last layer ($m = N$) by setting the first term to zero.

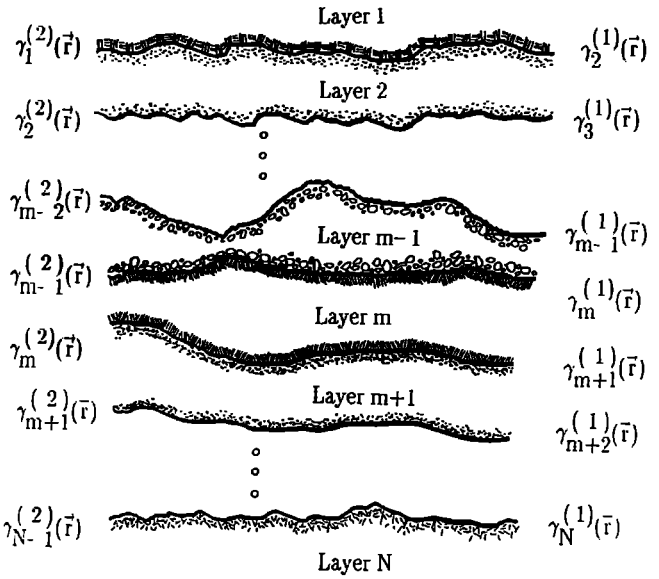

Fig. 1. A model consisting of N homogeneous layers.

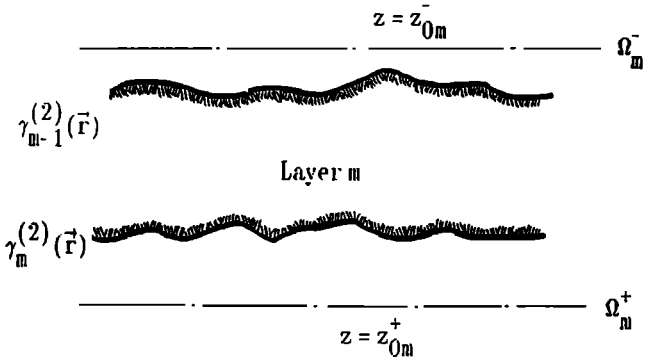

Fig. 2. Surfaces Ω_m^+ and Ω_m^- containing the source distributions which produce the scattered waves in layer m.

At each interface, $\Upsilon_1^{(2)}(\vec{r})$ through $\Upsilon_{N-1}^{(2)}(\vec{r})$, one boundary condition describes the continuity of pressure, and one boundary condition describes the continuity of the normal component of displacement (which, in this case, is equivalent to continuity of the normal derivative of pressure). This results in two equations at each of the N-1 interfaces. These equations may be written in general as

$$\iint_{\Omega_m^+} A_m^+(\vec{r}',\omega)\, G_m(\vec{r}\mid\vec{r}')\, d\Omega_m^+(\vec{r}') + \iint_{\Omega_m^-} A_m^-(\vec{r}',\omega)\, G_m(\vec{r}\mid\vec{r}')\, d\Omega_m^-(\vec{r}') = \iint_{\Omega_{m+1}^+} A_{m+1}^+(\vec{r}',\omega)\, G_{m+1}(\vec{r}\mid\vec{r}')\, d\Omega_{m+1}^+(\vec{r}') + \iint_{\Omega_{m+1}^-} A_{m+1}^-(\vec{r}',\omega)\, G_{m+1}(\vec{r}\mid\vec{r}')\, d\Omega_{m+1}^-(\vec{r}') \quad (2)$$

and

$$\iint_{\Omega_m^+} A_m^+(\vec{r}',\omega)\, \dot{G}_m(\vec{r}\mid\vec{r}')\, d\Omega_m^+(\vec{r}') + \iint_{\Omega_m^-} A_m^-(\vec{r}',\omega)\, \dot{G}_m(\vec{r}\mid\vec{r}')\, d\Omega_m^-(\vec{r}') = \iint_{\Omega_{m+1}^+} A_{m+1}^+(\vec{r}',\omega)\, \dot{G}_{m+1}(\vec{r}\mid\vec{r}')\, d\Omega_{m+1}^+(\vec{r}') + \iint_{\Omega_{m+1}^-} A_{m+1}^-(\vec{r}',\omega)\, \dot{G}_{m+1}(\vec{r}\mid\vec{r}')\, d\Omega_{m+1}^-(\vec{r}') \quad (3)$$

for all points, $\vec{r}$, on $\Upsilon_m^{(2)}(\vec{r})$ and for m = 1,2,3,....,N-1 and where $\dot{G}_m(\vec{r}\mid\vec{r}')$ represents the normal derivative of the Green's function at the point, $\vec{r}$, on the interface. Again on the last interface (m = N-1) the first term on the right-hand side of each of these equations will be zero. In the case of the first interface (m = 1) the second term on the left-hand side of each of these equations will be zero. The effect of placing a source in layer 1 can then be accommodated by adding $\Psi_0(\vec{r})$ and $\dot{\Psi}_0(\vec{r})$, respectively, to the left-hand sides of the preceding equations when m = 1. In this case, $\Psi_0(\vec{r})$ and $\dot{\Psi}_0(\vec{r})$ represent the incident wave's contribution to the pressure and its normal derivative on the interface $\Upsilon_1^{(2)}(\vec{r})$.

The net result (when all $N-1$ interfaces are considered) is a set of integral equations in which the source distribution functions $A_m^+(\vec{r}',\omega)$ and $A_m^-(\vec{r}',\omega)$ serve as the unknowns. Therefore, following the procedure commonly used in the method of moments [*Harrington*, 1968] and the boundary element method [*Brebbia*, 1978], sets of basis and testing functions are introduced. Each unknown source distribution function is represented as a linear combination of basis functions in accordance with

$$A_m^+(\vec{r}',\omega) = \sum_{v=1}^{K} a_{mv}^+(\omega)\, W_v(\vec{r}') \quad (4)$$

$$A_m^-(\vec{r}',\omega) = \sum_{v=1}^{K} a_{mv}^-(\omega)\, W_v(\vec{r}') \quad (5)$$

Multiplying each of the terms in the integral equations by the testing function $W_\mu^\dagger(\vec{r})$ and integrating the result over the appropriate interface, $\Upsilon_m^{(2)}(\vec{r})$, finally results in a system of simultaneous algebraic equations in which the linear combination coefficients, a_{mv}^+ and a_{mv}^- serve as the unknowns.

Furthermore, since the boundary conditions only couple the linear combination coefficients for adjacent layers, the overall system of equations is sparse and is, in fact, of the general form

$$\begin{bmatrix} \vec{\Gamma} \\ \vec{\Gamma} \\ 0 \\ \cdot \\ 0 \end{bmatrix} = \begin{bmatrix} U_1 & V_1 & 0 & \cdot & 0 \\ 0 & U_2 & V_2 & \cdot & 0 \\ 0 & 0 & U_3 & V_3 & \cdot \\ \cdot & \cdot & \cdot & \cdot & \cdot \\ 0 & \cdot & \cdot & U_{N-1} & V_{N-1} \end{bmatrix} \cdot \vec{a} \quad (6)$$

where
$\vec{a} = [a_{11}^{-}..a_{1K}^{-}\, a_{11}^{+}..a_{1K}^{+} \mid a_{21}^{-}..a_{2K}^{-}\, a_{21}^{+}..a_{2K}^{+} \mid \ldots \mid a_{N1}^{-}..a_{NK}^{-}\, a_{N1}^{+}..a_{NK}^{+}]^T$
and of course a_{11}^{-} through a_{1K}^{-} as well as a_{N1}^{+} through a_{NK}^{+} are zero. The left-hand side contains the effect of the incident wave upon the first interface. In particular,

$$\vec{\Gamma}_\mu = \iint_{\Upsilon_1^{(2)}} W_\mu^{\dagger}(\vec{r})\, \Psi_0(\vec{r})\, d\Upsilon_1^{(2)}(\vec{r}) \tag{7}$$

while

$$\vec{\Gamma}_\mu = \iint_{\Upsilon_1^{(2)}} W_\mu^{\dagger}(\vec{r})\, \Psi_0(\vec{r})\, d\Upsilon_1^{(2)}(\vec{r}) \tag{8}$$

Each of the submatrices (U_m and V_m for m = 1 to N-1) will generally be of full rank (2K x 2K). Physically, the U_m matrices represent the pressure (and its normal derivatives) at interface $\Upsilon_m^{(2)}(\vec{r})$ in layer m, while the V_m matrices represent the same quantities in layer m+1. Specifically, each U_m matrix can be partitioned into four matrices each having rank (K x K), i.e.,

$$U_m = \begin{bmatrix} -I_m^{(2)-} & -I_m^{(2)+} \\ -\dot{I}_m^{(2)-} & -\dot{I}_m^{(2)+} \end{bmatrix} \tag{9}$$

$$V_m = \begin{bmatrix} I_{m+1}^{(1)-} & I_{m+1}^{(1)+} \\ \dot{I}_{m+1}^{(1)-} & \dot{I}_{m+1}^{(1)+} \end{bmatrix} \tag{10}$$

where

$$I_{m\mu\nu}^{()\pm} = \iint_{\Upsilon_m^{()}} \iint_{\Omega_m^{\pm}} W_\mu^{\dagger}(\vec{r})\, G_m(\vec{r} \mid \vec{r}\,') \cdot W_\nu(\vec{r}\,')\, d\Omega_m^{\pm}(\vec{r}\,')\, d\Upsilon_m^{()}(\vec{r}) \tag{11}$$

and

$$\dot{I}_{m\mu\nu}^{()\pm} = \iint_{\Upsilon_m^{()}} \iint_{\Omega_m^{\pm}} W_\mu^{+}(\vec{r})\, \dot{G}_m(\vec{r} \mid \vec{r}\,') \cdot W_\nu(\vec{r}\,')\, d\Omega_m^{\pm}(\vec{r}\,')\, d\Upsilon_m^{()}(\vec{r}) \tag{12}$$

for μ = 1,2,3,...,K and ν = 1,2,3,...,K. The argument inside the superscript parentheses may be either 1 or 2.

Furthermore, since linear combination coefficients a_{11}^{-} through a_{1K}^{-} as well as a_{N1}^{+} through a_{NK}^{+} are all zero, arbitrary values could be assigned to the submatrix elements in $I_1^{(2)-}$, $\dot{I}_1^{(2)-}$, $I_N^{(1)+}$, and $\dot{I}_N^{(1)+}$ which multiply these particular combination coefficients without altering the values of the remaining (nonzero) combination coefficients. For this reason, an additional surface, Ω_1^{-} upon which $Z = Z_{01}^{-}$, is placed in layer 1 at some finite distance above $\Upsilon_1^{(2)}(\vec{r})$ and an additional surface, Ω_N^{+} upon which $Z = Z_{0N}^{+}$ is placed in layer N at some finite distance below $\Upsilon_N^{(1)}(\vec{r})$. By introducing these additional surfaces the preceding pair of equations for calculating individual matrix elements can be applied in all cases.

In order to solve the large set of equations which govern the combination coefficients while taking advantage of the sparse matrix form it is convenient to introduce the notation:

$$\vec{a}_m = [a_{m1}^{-} \cdots a_{mK}^{-}\, a_{m1}^{+} \cdots a_{mK}^{+}]^T \tag{13}$$

Thus, for any value of m between 2 and N-1, the coefficients, $\vec{a}_m$, for layer m can be expressed in terms of the coefficients for the underlying layer (layer m+1) as

$$\vec{a}_m = -U_m^{-1} \cdot V_m \cdot \vec{a}_{m+1} \tag{14}$$

By repeated application of this formula, the coefficients for layer 2 are related to those for layer N through

$$\vec{a}_2 = \left[\prod_{m=2}^{N-1} (-U_m^{-1} \cdot V_m)\right] \cdot \vec{a}_N \tag{15}$$

As previously stated, the first K elements of $\vec{a}_1$ and the last K elements of $\vec{a}_N$ are zero. Therefore, if $\vec{u} = \vec{a}_1 + \vec{a}_N$ and the matrices H^{+} and H^{-} are each 2K x 2K matrices defined by

$$H_{\mu\nu}^{+} = \begin{cases} \delta_{\mu\nu} & \text{for } 1 \le \mu \le K \text{ and } 1 \le \nu \le K \\ 0 & \text{otherwise} \end{cases} \tag{16}$$

and

$$H_{\mu\nu}^{-} = \begin{cases} \delta_{\mu\nu} & \text{for } K+1 \le \mu \le 2K \text{ and } K+1 \le \nu \le 2K \\ 0 & \text{otherwise} \end{cases} \tag{17}$$

the vectors $\vec{a}_1$ and $\vec{a}_N$ can be recovered from $\vec{u}$ by

$$\vec{a}_1 = H^{-} \cdot \vec{u} \quad \text{and} \quad \vec{a}_N = H^{+} \cdot \vec{u}$$

while the vector $\vec{u}$ can be found from

$$\vec{u} = \left\{ U_1 \cdot H^{-} + V_1 \cdot \left[\prod_{m=2}^{N-1} (-U_m^{-1} \cdot V_m)\right] \cdot H^{+} \right\}^{-1} \cdot \left[\vec{\Gamma} \mid \dot{\vec{\Gamma}}\right]^T \tag{18}$$

3. A SPECIAL CASE

These results are general and do not depend upon a particular choice of basis and testing functions. However, if we consider two-dimensional problems (in which neither the incident wave nor the interfaces vary in the y direction), it is sufficient to consider a set of basis functions which vary as a function of x alone since the basis functions describe the source distribution functions on surfaces of constant depth (z). In particular, we will consider the harmonically related complex sinusoids

$$W_\nu(\vec{r}) = \exp[ivk_0 x];$$
$$\nu = -\nu_0, -\nu_0+1, \cdots -1, 0, 1, \cdots \nu_0-1, \nu_0 \tag{19}$$

as the set of basis functions and

$$W_\mu^{\dagger}(\vec{r}) = \exp[-i\mu k_0 x];$$
$$\mu = -\nu_0, -\nu_0+1, \cdots -1, 0, 1, \cdots \nu_0-1, \nu_0 \tag{20}$$

as the set of testing functions.

The pressure field produced by a source distribution function of $W_\nu(\vec{r})$ acting on the surface $\Omega_m^{\pm}$ at $Z = Z_{0m}^{\pm}$ is given by the integral:

$$P_{m\nu}(\vec{r}, \omega) = \iint_{\Omega_m^{\pm}} W_\nu(\vec{r}\,')\, G(\vec{r} \mid \vec{r}\,')\, d\Omega_m^{\pm}(\vec{r}\,') \tag{21}$$

or, equivalently by the solution of the inhomogeneous acoustic wave equation

$$[\nabla^2 + (\omega^2/c_m^2)] P_{m\nu}(\vec{r}) = -\exp[ivk_0 x]\delta(Z - Z_{0m}^{\pm}) \tag{22}$$

Writing $P_{m\nu}(\vec{r}, \omega)$ as

$$P_{m\nu}(\vec{r}, \omega) = F_m(z) \exp[i\nu k_0 x] \quad (23)$$

substitution of this expression for $P_{m\nu}$ into the wave equation results in the ordinary differential equation:

$$\left[\frac{d^2}{dZ^2} + \left(\frac{\omega^2}{c_m^2} - \nu^2 k_0^2\right)\right] F_m(Z) = -\delta(Z - Z_{0m}^{\pm}) \quad (24)$$

having as its solutions

$$F_m(z) = \begin{cases} A \exp[iq_{m\nu}(Z - Z_{0m}^{\pm})] \\ \quad + B \exp[-iq_{m\nu}(Z - Z_{0m}^{\pm})] \text{ for } Z \le Z_{0m}^{\pm} \\ C \exp[iq_{m\nu}(Z - Z_{0m}^{\pm})] \\ \quad + D \exp[-iq_{m\nu}(Z - Z_{0m}^{\pm})] \text{ for } Z > Z_{0m}^{\pm} \end{cases} \quad (25)$$

where

$$q_{m\nu} = \sqrt{(\omega/c_m)^2 - \nu^2 k_0^2}$$

The radiation condition then requires A = D = 0. Furthermore, continuity of $F_m(z)$ at $Z = Z_{0m}^{\pm}$ is ensured by setting B = C. Finally, applying the jump condition at $Z = Z_{0m}^{\pm}$

$$\begin{aligned} &\underset{\varepsilon\to 0}{Limit}\left\{\frac{d}{dz}F_m(Z)\Big|_{Z=Z_{0m}^{\pm}-\varepsilon} - \frac{d}{dz}F_m(Z)\Big|_{Z=Z_{0m}^{\pm}+\varepsilon}\right\} \\ &= C(iq_{m\nu}) - B(-iq_{m\nu}) = 2C(iq_{m\nu}) \\ &= \underset{\varepsilon\to 0}{Limit}\int_{Z_{0m}^{\pm}-\varepsilon}^{Z_{0m}^{\pm}+\varepsilon} -\delta(Z - Z_{0m}^{\pm}) = -1 \end{aligned} \quad (26)$$

Thus B = C = $i/2q_{m\nu}$ which in turn allows the pressure function $P_{m\nu}(\vec{r}, \omega)$ to be written as:

$$P_{m\nu}(\vec{r}, \omega) = \frac{i}{2q_{m\nu}} \exp[i\nu k_0 x] \exp[iq_{m\nu} | Z - Z_{0m}^{\pm} |] \quad (27)$$

This result, apart from minor differences in notation and the restriction to two dimensions, agrees with the Weyl expansion of a spherical wave in terms of plane waves [*Aki and Richards*, 1980], as it should on the basis of equation (21).

By combining this particular set of harmonically related basis functions with a piecewise linear model of the reflector surface as shown in Figure 3 it can be shown that all of the matrix elements can be expressed in closed form. In particular, it is assumed that each reflector consists of L-1 straight-line segments. Thus the endpoints of segment n of the reflector $\Upsilon_m^{(2)}(\vec{r})$ are, for example, $(X_n, Z_{mn}^{(2)})$ and $(X_{n+1}, Z_{mn+1}^{(2)})$. The downward normal to this segment is presumed to form an angle of θ with respect to the vertical direction (z axis). Denoting the cosine, sine, and tangent of θ as $t_{mn}^{(2)}$, $s_{mn}^{(2)}$, and $\delta_{mn}^{(2)}$, respectively, allows us to define the functions

$$\Phi_{mn\mu\nu}^{(1)-} = (\nu - \mu)k_0 + q_{m\nu}\delta_{mn}^{(1)} \quad (28)$$

$$\Phi_{mn\mu\nu}^{(2)-} = (\nu - \mu)k_0 + q_{m\nu}\delta_{mn}^{(2)} \quad (29)$$

$$\Phi_{mn\mu\nu}^{(1)+} = (\nu - \mu)k_0 - q_{m\nu}\delta_{mn}^{(1)} \quad (30)$$

$$\Phi_{mn\mu\nu}^{(2)+} = (\nu - \mu)k_0 - q_{m\nu}\delta_{mn}^{(2)} \quad (31)$$

This, in turn, allows the matrix elements to be written as

$$I_{m\mu\nu}^{(\ )\pm} = \sum_{n=1}^{L-1} F_{mn\mu\nu}^{(\ )\pm} \quad (32)$$

and

$$\dot{I}_{m\mu\nu}^{(\ )\pm} = \sum_{n=1}^{L-1} \dot{F}_{mn\mu\nu}^{(\ )\pm} \quad (33)$$

where the argument in the parentheses is 1 for the upper boundary of layer m and 2 for the lower boundary.

The summands, $F_{mn\mu\nu}^{(\ )\pm}$ and $\dot{F}_{mn\mu\nu}^{(\ )\pm}$ may then be shown to be

$$F_{mn\mu\nu}^{(\ )\pm} = \frac{\exp[\pm iq_{m\nu}(Z_{0m}^{\pm} - Z_{mn}^{(\ )} + \delta_{mn}^{(\ )} X_n)]}{2q_{m\nu}t_{mn}^{(\ )}\Phi_{mn\mu\nu}^{(\ )\pm}} \cdot \left\{\exp[i\Phi_{mn\mu\nu}^{(\ )\pm} X_{n+1}] - \exp[i\Phi_{mn\mu\nu}^{(\ )\pm} X_n]\right\} \quad (34)$$

and

$$\dot{F}_{mn\mu\nu}^{(\ )\pm} = F_{mn\mu\nu}^{(\ )\pm}[i\nu k_0 s_{mn}^{(\ )} - (\pm iq_{m\nu}t_{mn}^{(\ )})] \quad (35)$$

in general. However, when segment n is horizontal, $\delta_{mn}^{(\ )} = 0$ which causes $\Phi_{mn\mu\nu}^{(\ )\pm} = 0$ whenever $\mu = \nu$. Under this condition the relation between $F_{mn\mu\nu}^{(\ )\pm}$ and $F_{mn\mu\nu}^{(\ )\pm}$ remains unchanged, but the expression for $\dot{F}_{mn\mu\nu}^{(\ )\pm}$ should be replaced with

$$F_{mn\mu\nu}^{(\ )\pm} = \frac{i \exp[\pm iq_{m\mu}(Z_{0m}^{\pm} - Z_{mn}^{(\ )} + \delta_{mn}^{(\ )} X_n)]}{2q_{m\nu}t_{mn}^{(\ )}} \cdot [X_{n+1} - X_n] \quad (36)$$

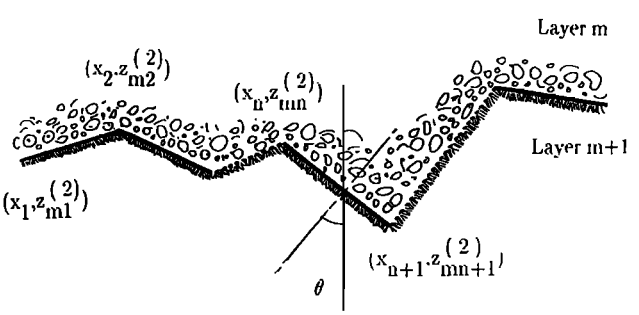

Fig. 3. The interface between layers m and m+1 as a sequence of line segments.

In this special case, the formulation is very similar to the method discussed by *Aki and Larner* [1970]. In the present method, weighted integrals are performed over the actual interface (equations (11) and (12)) rather than using a spartial Fourier transformation along the horizontal direction.

One of the inherent drawbacks of applying methods of this sort in the case of corrugated boundaries adjacent to a half-space is that the wavefield within the half-space consists of a summation of waves propagating away from the boundary. In the case of a source-free half-space below the interface, for example, the waves simulated by this method would all propagate in the downward direction. However, in the vicinity of the corrugated interface some of the waves in the half-space may be propagating locally in the upward direction. This difficulty is referred to as the Rayleigh ansatz error [*Aki and Larner*, 1970; *Aki and Richards*, 1980].

As in the wavenumber coupling method described by [*Aki and Larner*, 1970], the error may preclude complete determination of the wave-induced pressure fluctuations in the vicinity of the corrugated boundary. However, in the examples which follow the waves will be simulated on a horizontal datum plane which is located above the interface.

4. Results and Discussion

In order to check this method, synthetic seismograms were generated for a number of simple single-interface geological models. In the case of a flat horizontal interface, subjected to an incident plane wave, for example, the results were in agreement with the known analytical solution.

The next geological model to be considered was a V shaped reflector having the geometry shown in Figure 4.

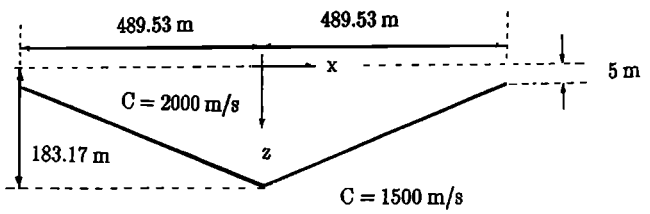

Fig. 4. A simple single reflector model.

Two types of incident waves were considered. In the first case the incident wave was specified as a vertically propagating plane wave, while in the second case the incident wave was specified as the wave which would be produced by a line source oriented parallel to the y axis.

The synthetic seismograms generated in this way were then used as the input data for a migration process described in an earlier paper [*DuBroff*, 1986] in order to see if the reflector geometry and the acoustic wave speed below the reflector could be reconstructed from this type of synthetic data.

The various parameters which were used in generating the synthetic data for both cases are summarized in Table 1. The parameter ξ was used to introduce a small amount of attenuation. This was found to be helpful in reducing the severity of spatial aliasing which results from the spatial harmonic relation between the basis functions.

A qualitative explanation of the effects of spatial aliasing is provided by reference to Figure 5 and 6. Figure 5*a*, for example, shows the horizontal dependence of the real part of the kernel function $G_m(\vec{r} \mid \vec{r}')$ when $\vec{r}' = 0$ and when $\vec{r}$ varies along a horizontal line (parallel to the x axis) located 40 m below the point $\vec{r} = 0$. Figure 5*a* (and figures 5*b*, 6*a*, and 6*b*) was based upon a frequency 21 Hz, a wave speed of 2000 m/s, a model width of L = 979.06 m, and no attenuation. Note that the kernel function has a central peak flanked by smaller oscillations. The envelope of the

TABLE 1. Parameters Used for Generating Synthetic Seismograms

Parameter	Plane wave	Line Source
# geophones	32	32
sampling interval(sec)	.005	.005
geophone spacing	31.58	31.58
# time samples	75	75
x coordinate of source	*	0
z coordinate of source	*	-200
z coordinate of geophones	0	-200
attenuation (ξ)	3	4
lowest frequency (Hz)	10.667	10.667
highest frequency (Hz)	32.00	40.00
starting time (sec)	0	0.100

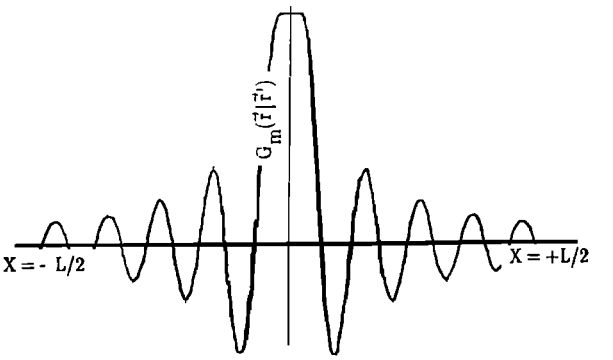

Fig. 5*a*. Kernel function along a horizontal surface 40m deep.

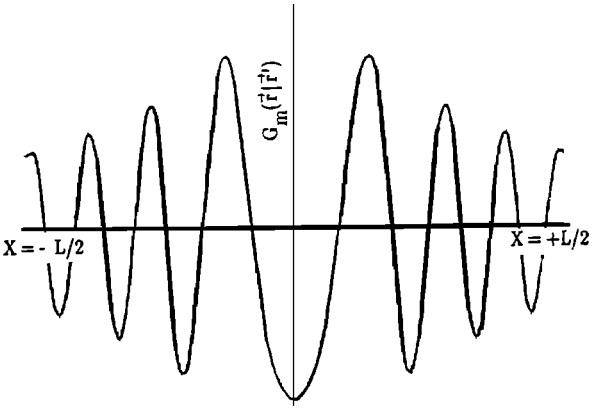

Fig. 5*b*. Kernel function along a horizontal surface 200m deep.

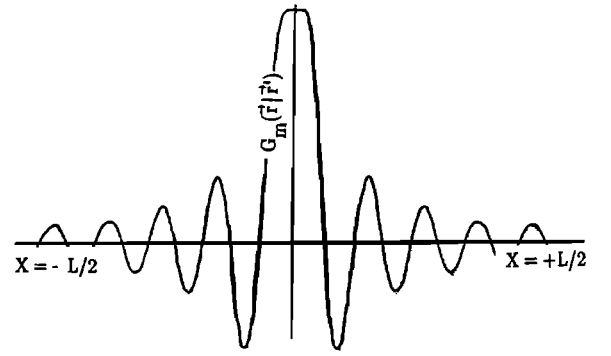

Fig. 6*a*. Effect of aliasing on Figure 5*a*.

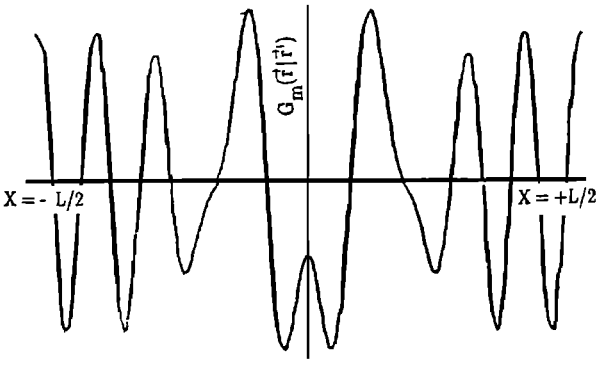

Fig. 6*b*. Effect of aliasing on Figure 5*b*.

oscillations is relatively narrow. Figure 5*b* was obtained by considering a horizontal line 200 m below the point $\bar{r}' = 0$, while leaving all other parameters unchanged. The envelope of the kernel function is considerably smoother when compared to the function shown in Figure 5*a*.

In the special case of harmonically related sinusodal basis and testing functions, the increment in horizontal wave number between any two consecutive basis function is $2\pi / L$. Therefore the kernel function will, in effect, be aliased. To demonstrate this, Figure 6*a* and 6*b* were obtained from Figure 5*a* and 5*b*, respectively, by adding the aliasing terms $G_m(\bar{r} \mid L\hat{x})$ and $G_m(\bar{r} \mid -L\hat{x})$.

Of course, there will also be additional higher-order aliasing terms, but Figure 6*a* and 6*b* suffice to demonstrate the cause of this difficulty. In comparing Figure 5*a* with Figure 6*a* the difference between the two figures is a relatively insignificant fraction of the peak value at X = 0. On the other hand, when the kernel function envelope becomes smoother (as in Figure 5*b*) the aliasing becomes more significant (Figure 6*b*). Results in these highly aliased cases have shown that the simulated seismic response may appear chaotic and unstable, bearing no resemblance to the correct response.

Including attenuation has the effect of sharpening the kernel function thereby reducing the aliasing and improving the quality of the simulated time sections. Similar improvements can also be obtained by increasing the model width. However, improvements obtained in this manner tend to be more expensive in terms of increasing the number of basis function combination coefficients which need to be determined simultaneously. Also, attenuation causes the sides of the kernel function to decay exponentially while increasing the model width only causes an algebraic decay factor of r^{-1} in three dimensions or $r^{-1/2}$ in two dimensions. The amount of attenuation used in these examples is relatively small and satisfies the condition $\xi << \omega$.

The inclusion of attenuation is accommodated by an additional term of the form $(i\xi\omega/c_m^2)\, P_{mv}$ on the left side of equation (22) [see *Berkhout*, 1980]. Also, in the line source case the cylindrical incident wave produced by the line source was modified by the removal of all plane wave components having horizontal wavenumbers greater than ω/c_1. Although this may have some additional benefit in terms of decreasing spatial aliasing [*Nautiyal*, 1988; *Berkhout and Van Wulfften Pathe*, 1979], these components would have attenuated in any case as the incident wave progressed vertically downward. An additional possible cause for concern is the possibility. In this case, the system of equations which determine the combination coefficients becomes ill-conditioned. As an example, this type of instability may be associated with resonance frequencies [*Kleinman and Martin*, 1988; *Morita*, 1979]. Although the examples considered in this paper have not demonstrated any numerical instability in the solution of the resulting system of linear equations, this instability may become significant for more complex geometries such as inclusions, having closed boundaries. In any case, it is recommended that the error flags generated by the linear equation solving subroutines should be checked to ensure that the linear combination coefficients are not unduly sensitive to noise or round off errors.

The synthetic seismograms for the reflected waves are shown in Figure 7 for the case of a plane wave source and in Figure 8 for the case of a line source. Figure 7 and Figure 8 both demonstrate pressure fluctuations prior to the first arrival of the reflected wave. This is a consequence of having formulated the method in the frequency domain at a finite number of discrete equally spaced frequencies. The frequency spacing in this case is

$$\Delta f = \frac{1}{75 \times 0.005} = 2.67 \text{ Hz}$$

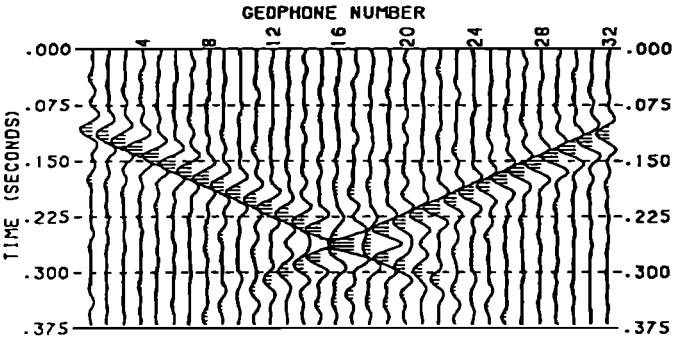

Fig. 7. Seismic response from a plane wave source.

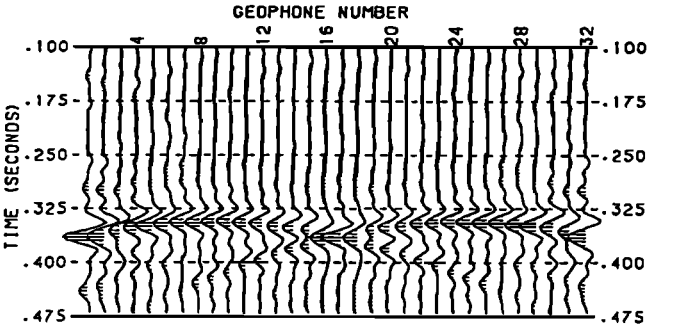

Fig. 8. Seismic response from a line source.

The implication is that the pressure response in the time domain will be periodic with a period of

$$T = \frac{1}{2.67} = 0.375 \text{ s}$$

Thus the apparent acausal response in figure 7 and 8 actually coresponds to the tails of the bandlimited wavelets from the previous time period. Figure 9 shows the image of the reflector computed from the former data (Figure 7) while Figure 10 shows the image of the reflector computed from the latter data (Figure 8). In both figure 9 and 10 the positive portions have been clipped off. Table 2 indicates the acoustic wave speed calculated for the lower half-space at points directly below the sensors (geophones). The results obtained in the first case (plane wave source) are very similar to the results shown by *DuBroff* [1986, 1988]. Actually, the data used in this earlier paper were also generated by the method described in the present paper except that a somewhat different integration scheme was used to calculate the matrix elements.

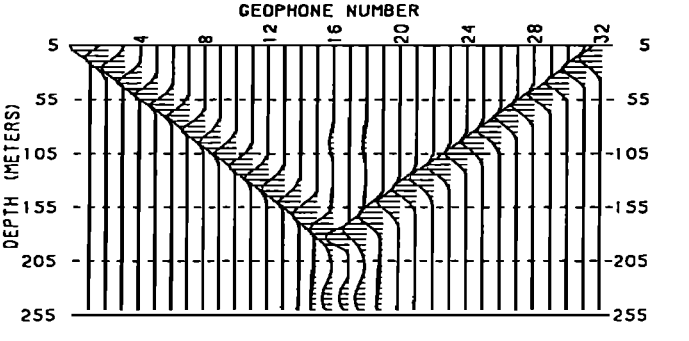

Fig. 9. Reconstruction of reflector from plane wave source data.

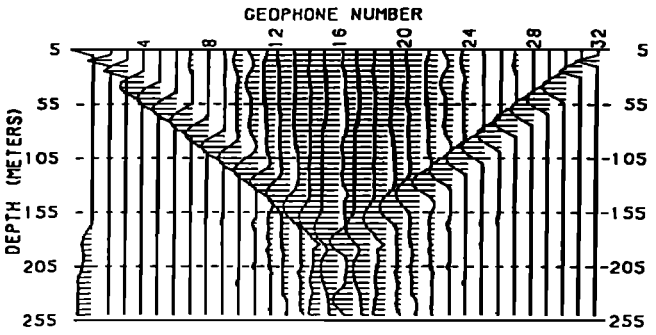

Fig. 10. Reconstruction of reflector from line source data.

TABLE 2. Estimated Wavespeeds Below Each Geophone in Layer 2

Geophone number	Plane wave	Line source
1	1555	1964
2	1568	983
3	1533	1244
4	1513	1006
5	1530	1054
6	1558	1045
7	1554	1279
8	1568	1406
9	1571	1365
10	1575	1308
11	1589	1413
12	1622	1314
13	1596	1485
14	1588	1589
15	1595	1682
16	1655	1564
17	1607	1562
18	1655	1564
19	1595	1682
20	1588	1589
21	1596	1485
22	1622	1314
23	1589	1412
24	1575	1308
25	1571	1365
26	1568	1406
27	1554	1279
28	1558	1045
29	1530	1054
30	1513	1007
31	1533	1245
32	1568	983

In comparing these two cases, it is clear that the results from the first case are superior to the results from the second case. This is particularly true for the estimated wave speeds in Table 2 near the sides of the model where the spatial aliasing effects would tend to be the most severe. Although some of this discrepancy is clearly the result of limitations in the modeling program, it should also be noted that the particular acoustic imaging algorithm being used to generate the depth sections is dependent upon the assumption that the acoustic waves can be regarded as being locally plane waves. This assumption is more likely to be satisfied in the first case than in the second as the distance between the line source and the reflector is of the order of one wavelength when the line source is used.

Although there are many other ways to select the basis functions and the testing functions, experience with these particular examples has shown that the parameters must be chosen carefully if one is to avoid the effects of spatial aliasing.

As is the case in most numerical schemes there are bound to be certain inherent errors. In addition to the previously mentioned sources of error it should also be noted that corners on the reflector (such as the one occurring at the vertex of the V-shaped reflector) can not be completely represented as the normal derivative appearing in equation (3) is not defined where the slope of the reflector changes discontinuously. In this method the discontinuity is smoothed out by performing weighted integrals.

Nevertheless, the examples considered have demonstrated sufficient accuracy to allow a reasonable image of the reflector to be reconstructed and seem to be in general qualitative agreement with the expected results.

NOTATION

$A_m^{\pm}(\vec{r}', \omega)$ source distribution functions for layer m.
c_m acoustic wavespeed in layer m.
$G_m(\vec{r} \mid \vec{r}')$ Green's function for layer m.
K total number of basis (testing) functions.
$W_\nu(\vec{r})$ νth basis function.
$W_\mu^\dagger(\vec{r})$ μth testing function.
$(x_n, Z_{mn}^{(1,2)})$ coordinates of the nth vertex on the lower (upper) boundary of layer m.
$\Upsilon_m^{(1,2)}(\vec{r})$ upper and lower boundaries of layer m.
$\Psi_0(\vec{r})$ incident wave.
$\Omega_m^{\pm}$ auxiliary surfaces above and below layer m.

Acknowlegment. Acknowledgment is made to the donors of the Petroleum Research Fund, administered by the American Chemical Society for support of this research.

REFERENCES

Aki, K., and K. L. Larner, Surface motion of a layered medium having an irregular interface due to incident plane *SH* waves, *J. Geophys. Res., 75*(5), 933-953, 1970.

Aki, K., and P. G. Richards, *Quantitative Seismology,* vol. 1, W. H. Freeman, New York, 1980.

Berkhout, A. J., *Seismic Migration Imaging of Acoustic Energy by Wavefield Extrapolation,* Elsevier Scientific, New York, 1980.

Berkhout, A. J. , and D. W. Van Wulfften Palthe, Migration in terms of spatial deconvolution, *Geophys. Prospect., 27*(1), 261-291, 1979.

Brebbia C. A., *The Boundary Element Method for Engineers,* John Wiley, New York, 1978.

Claerbout, J. F., *Fundamentals of Geophysical Data Processing With Applications to Petroleum Prospecting,* McGraw-Hill, New York, 1976.

DuBroff, R. E., Acoustic imaging and the juxtaposition of waves, *J. Geophys. Res., 91*(B3), 3784-3794, 1986.

DuBroff, R. E., Boundary element-image method simulation of seismic waves, paper presented at 1988 Fall Meeting, AGU, San Francisco, Calif., Dec. 5-9, 1988

Harrington, R. F., *Field Computation by Moment Methods,* reprinted by Roger F. Harrington, Cazenovia, N. Y., 1968.

Kelly K. R., S. W. Ward, S. W. Treitel, and R. M. Alford, Synthetic seismograms a finite difference approach, *Geophysics 41,* 2-27, 1978.

Kleinman, R. E., and P. A. Martin, On single integral equations for the transmission problem of acoustics, *SIAM J. Appl. Math., 48*(2), 307-325, 1988.

Leviatan, Y., A. Boag, and A. Boag, Analysis of TE scattering from dielectric cylinders using a multifilament

magnetic current model, *IEEE Trans. Antennas Propag.*, vol. 36, 1026-1031, 1988.

Marfurt, K. J., Accuracy of finite-difference and finite-element modeling of the scalar and elastic wave equations, *Geophysics, 49*(5), 533-549 1984.

Morita, N., Resonant solutions in the integral equation approach to scattering from conducting and dielectric cylinders, *IEEE Trans. Antennas Propagat., AP-27,* 869-871, 1979.

Nautiyal, A. Antialiasing methods for two-dimensional spatial wavelets in seismic modeling, *Geophysics, 539,* 1202-1206, 1988.

Schuster, G. T., and L. C. Smith, A comparison among four direct boundary integral methods, *J. Acoust. Soc. Am., 77,* 850-864, 1985.

Zienkiewicz, O. C., *The Finite Element Method* 3rd ed., McGraw-Hill, New York, 1977.

R. E. DuBroff, Department of Electrical Engineering, University of Missouri at Rolla, Rolla, MO 65401.

(Received February 17, 1989
revised September 22, 1989
accepted September 7, 1989.)